



Study on the abrasive retention capacity on the surface of electroplated diamond wire saw

Jintao Zheng¹ · Qian Xie¹ · Peiqi Ge^{1,2} · Jianfeng Meng^{1,2} · Wenbo Bi^{1,2}

Received: 19 March 2021 / Accepted: 15 June 2021 / Published online: 24 June 2021
© The Author(s), under exclusive licence to Springer-Verlag London Ltd., part of Springer Nature 2021

Abstract

The quality and efficiency of slicing will be reduced if the abrasives on the surface of a diamond wire saw shed in sawing. Generally, the diamond abrasives are held on the surface of an electroplated diamond wire saw by a nickel-plated layer. The abrasive retention state, reflecting abrasive shedding, can be characterized by the plastic deformation of the plating layer at the interface between the nickel-plated layer and the abrasive. To gain an in-depth understanding of the abrasive shedding mechanism, a finite element model that the double-cone diamond abrasive is embedded in a nickel-plated layer was established based on the mechanical properties test of the nickel-plated layer in this paper to research the effects of the residual stress and hardness of the nickel-plated layer as well as the protrusion height of the diamond abrasive on the abrasive retention capacity. The results show that the residual stress on the surface layer of the nickel-plated layer was compressive stress. The abrasive retention capacity was increased with the increase of the hardness or the decrease of the residual compressive stress of the nickel-plated layer. For the same diamond abrasive, it was decreased with the increase of the protrusion height of the abrasive. Based on the results of the finite element analysis, a calculation procedure of abrasive shedding rate was presented. Subsequently, the slicing experiment of a single crystal silicon rod was carried out by the Meyer Burger RTD6800 multi-wire sawing machine and the electroplated diamond wire saw with a core wire diameter of 65 μm. The abrasive shedding rate of the diamond wire saw caused by sawing was analyzed theoretically and experimentally. The research work is of great significance to improve the quality detection and evaluation of an electroplated diamond wire saw.

Keywords Electroplated diamond wire saw · Abrasive retention capacity · Wire saw slicing · Abrasive shedding

1 Introduction

An electroplated diamond wire saw is widely employed for the sawing of brittle materials due to its high sawing efficiency, low environmental pollution, and low production and manufacture costs [1–3]. With the development of photovoltaic silicon slicing technology, there are higher and higher requirements for the performance of a diamond wire saw [4]. Generally, in the production process of the electroplated diamond wire saw, the diamond abrasives are deposited on the

surface of metal wire by composite electroplating [5], and then attached by a nickel-plated layer. Therefore, the mechanical properties of the nickel-plated layer have a significant effect on the abrasive retention capacity on the surface of the diamond wire saw which is the ability of the nickel-plated layer to bond the diamond abrasive and prevent it from shedding. In the sawing process of crystal material with the diamond wire saw, the removal of the workpiece material is achieved by the scratching of the diamond abrasive. The abrasive shedding caused by sawing force will reduce the quality and efficiency of slicing, and even lead to the wear failure of the diamond wire saw. Therefore, the abrasive retention capacity on the surface of the electroplated diamond wire saw is a key factor that affects its working performance.

Generally, the abrasive retention capacity of nickel mainly depends on the chemical and mechanical action of the interface between them. The former makes the diamond abrasive adhered by the chemical bond formed between diamond abrasive and nickel [6, 7], while the latter prevents the diamond

✉ Peiqi Ge
pqge@sdu.edu.cn

¹ School of Mechanical Engineering, Shandong University, Jinan 250061, China

² Key Laboratory of High-Efficiency and Clean Mechanical Manufacture at Shandong University, Ministry of Education, Jinan 250061, China

abrasive from shedding by the mechanical occlusion [8]. For the electroplated diamond wire saw shown in Fig. 1, the attachment of the diamond abrasives mainly depends on the occlusion effect of the nickel-plated layer. Therefore, the mechanical binding force plays a more important role for the nickel-plated layer to hold the diamond abrasives, which is the focus of this paper.

The quantitative characterization methods of the abrasive retention capacity mainly include analysis on bending strength and calculation by elasticity equation [9]. However, in order to improve the sawing ability of a diamond wire saw, only the characterization of the abrasive retention capacity cannot meet the needs of engineering, so it is necessary to study the mechanism of diamond abrasive shedding. Webb [10] proposed the diamond abrasive retention R , which reflects the relationship between the forces of diamond abrasives participating in sawing. The research shows that only when the R value is greater than 1, the diamond abrasive can be well held on the metal substrate. Xu et al. [11] believed that the abrasive shedding was caused by the interface debonding between the diamond abrasive and the metal-plated layer. When the interface separation gap reaches a certain degree, the abrasive will shed. Besides that, it has been observed that the shapes and orientations of diamond abrasives and the interfacial properties have a significant influence on the abrasive retention capacity. Romanski [8] reported that the abrasive shedding was caused by the deformation of the metal-plated layer embedded with the diamond abrasive. As shown in Fig. 2, one side of the plating layer embedded with the diamond abrasive will be squeezed by the loaded abrasive. And when the deformation of the plating layer reaches a certain value, there will be a large gap between the plating layer and the diamond abrasive, which makes the abrasive shed. According to Romanski's research, Konstany et al. [12] analyzed the influence of the different loading methods for diamond abrasive and the types

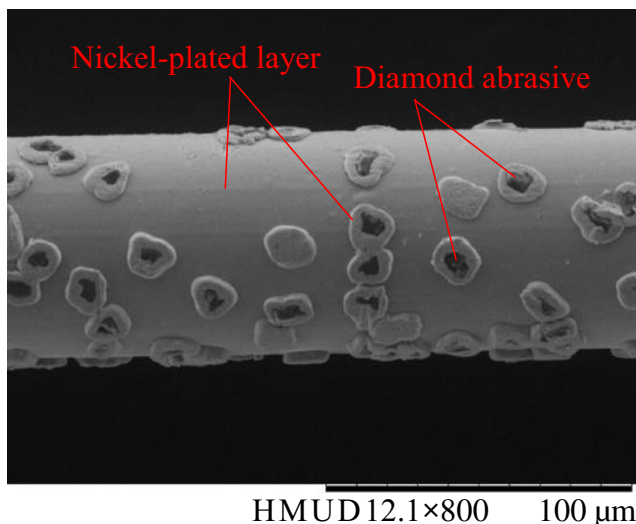


Fig. 1 Morphology of electroplated diamond wire saw

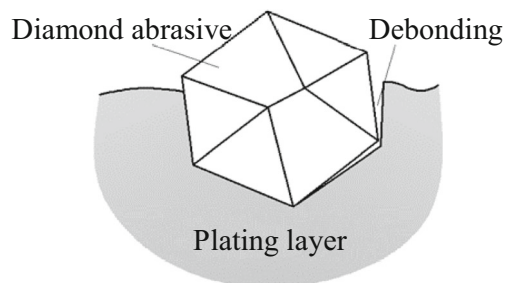


Fig. 2 Schematic diagram of diamond abrasive shedding

of the plating layer materials on the diamond abrasive shedding and considered that if the deformation of the plating layer reaches 4–8%, the diamond abrasive will be in the critical shedding state.

Up to now, the previous research works mainly focus on the evaluation of the abrasive retention capacity, but the study on the influences of the properties of the plating layer material embedded with the diamond abrasive on the abrasive retention capacity is relatively insufficient. In this paper, a finite element model was established to study the influences of the residual compressive stress and hardness of the nickel-plated layer as well as the abrasive protrusion height on the abrasive retention capacity of the electroplated diamond wire saw. Based on these, a simulation procedure was presented to calculate the theoretical abrasive shedding rate of the diamond wire saw after use. The reliability of the analysis method was verified by the single crystal silicon sawing experiment. This research will provide some guidance for the manufacture of an electroplated diamond wire saw.

2 Mechanical properties test of nickel-plated layer

2.1 Sample preparation

The abrasive retention capacity of an electroplated diamond wire saw is significantly related to the mechanical properties of the nickel-plated layer on its surface, including residual stress and hardness. Since the electroplated diamond wire saw is ultra-fine, it is difficult to directly measure the mechanical properties of the nickel-plated layer. Additionally, the mechanical properties are associated with the internal grain size of the nickel-plated layer which is mainly affected by the material properties and surface state of the substrate at the beginning of the formation of the nickel-plated layer rather than its shape and structure. Therefore, a T9A steel plate with similar chemical composition and mechanical properties to the core wire of an electroplated diamond wire saw is selected as the substrate to prepare the nickel-plated layer sample without diamond abrasive. The electroplated specimen with

dimensions of 100×40×6mm is obtained. The structure of electroplating experiment equipment is shown in Fig. 3.

In order to make the mechanical properties of the nickel-plated layer of the specimen consistent with those on the surface of the actual electroplated diamond wire saw, the process of electroplating is set as follows: removing oil by alkali washing, activating by acid washing, plating A layer, plating B layer, and plating C layer. The nickel-plated layers A, B, and C correspond to pre-plating, sanding, and thickening in the production process of an electroplated diamond wire saw, respectively. According to the actual production process parameters of the electroplated diamond wire saw with a core wire diameter of 65μm in industry, including constant temperature and PH value as well as cathode current density, the main parameters of electroplating experimental are set as shown in Table 1. In the experiment, the constant temperature of electroplating solution is controlled at 50°C, and the nickel-plated layers A, B, and C with the thickness of 0.1μm, 1.5μm, and 1.6μm respectively are obtained.

2.2 Measurement of residual stress in nickel-plated layer

The residual stress in the nickel-plated layer is measured by the X'Pert Pro MPD instrument in Holland. Because the residual stress in the material is associated with the change of crystal plane spacing, the lattice strain caused by the stress is consistent with the macroscopic strain calculated according to the elastic theory under a certain stress state [13]

$$\varepsilon_{\varphi\omega} = \frac{1}{2}S_2^{hkl} \sigma_{\varphi} \sin^2\psi + \sum \sigma_{ij} S_1^{hkl} \tag{1}$$

where $1/2S_2^{hkl}$ and S_1^{hkl} are X-ray elastic constants, (φ, ψ) is the azimuth of the measuring direction in the sample coordinate system, σ_{φ} and $\varepsilon_{\varphi\psi}$ are the lattice stress and strain in the measuring direction, respectively, and σ_{ij} is the component related to stress. In the measurement process, the lattice strain is expressed by the slip distance of the crystal plane $D_{spacing}$. When $D_{spacing} \sim \sin^2\psi$ is linear, the stress value can be obtained by the slope of the straight line, and a positive slope indicates compressive stress whereas a negative slope indicates tensile stress. In this paper, the relationship between $D_{spacing}$ and

$\sin^2\psi$ of the sample is shown in Fig. 4. The measured results are fitted by the linear fitting method, and it is obtained that the residual compressive stress is 601.6MPa.

2.3 Measurement of hardness of nickel-plated layer

The hardness and elastic modulus of the nickel-plated layer are measured by Fischer's HM200S nano hardness tester. The standard pyramid Vickers indenter is used for measurement in which the maximum load is set at 5mN and the loading time is 5s. The load-displacement curve is shown in Fig. 5. Subsequently, 4 points are measured on each specimen, and the mean value is taken as the effective hardness value of the nickel-plated layer. It is obtained that the surface elastic modulus and Vickers hardness are 166.6GPa and 3483MPa, respectively. According to Tabor's research results [14], the relationship between Vickers hardness and yield stress can be expressed as

$$HV = 2.9\sigma_s \tag{2}$$

where HV is Vickers hardness and σ_s is yield stress. According to Eq. (2), the yield stress of the nickel-plated layer is 1201MPa.

3 Finite element model

3.1 Model of diamond abrasive and nickel-plated layer

Although the primary diamond crystal is the octahedron, the abrasives adhered on the surface of an electroplated diamond wire saw are the crushed diamond crystal, most of which are pyramidal in shape. And it is found that most of the cutting edge shapes of abrasives with sawing effect are triangular pyramid by scanning the three-dimensional shapes of diamond abrasives on the surface of the diamond wire saw with a laser microscope. The measurement results of the abrasive geometry give the average angles of $\alpha_f = 66^\circ$ for the face angle, $\alpha_r = 76^\circ$ for the ridge angle, and $\alpha_w = 112^\circ$ for the wedge angle [15]. To simplify the calculation of the sawing force of the diamond abrasive cutting edge, the diamond

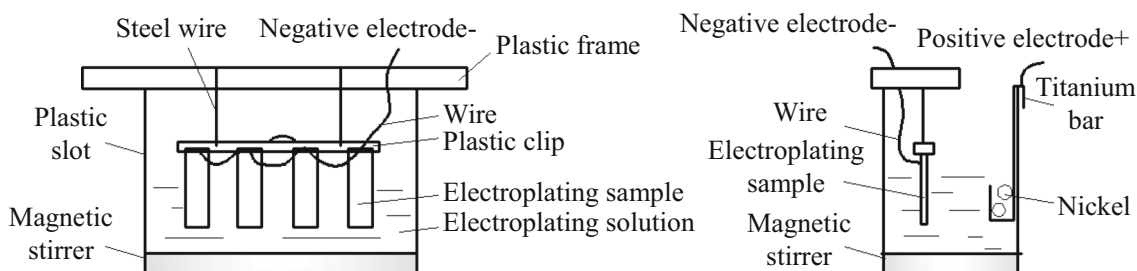


Fig. 3 Structure of electroplating experiment equipment

Table 1 Main process parameters of electroplating experiment

Process	PH value	Cathode current density (A/dm ²)	Electroplating time (s)
A	3.8	7.9	4
B	4.8	27.3	18
C	3.8	27.3	18

abrasive tip can be regarded as an equivalent conical tip with the average half-included angle $\psi_a = 76.903^\circ$ [16]. On the other hand, due to the strong randomness of the shape of the abrasive, only a similar geometric body can be used for modeling in the theoretical analysis process. Therefore, considering the overall shape of the abrasive and the simplification of the model, the abrasive is assumed to be the double-cone as shown in Fig. 6, so that its overall structure and extrusion effect on the nickel-plated layer are similar to most of the actual abrasives. According to the above, the double-cone diamond abrasive model with a diameter of 10 μm and an average half-included angle of 76.903° is established in this paper and the abrasive protrusion height accounts for about 1/3 of its diameter. The size of the nickel-plated layer embedded with the diamond abrasive is much larger than the diameter of the abrasive, and its material properties are consistent with the results measured in the previous section, as shown in Table 2.

In the finite element model, the contact type between the diamond abrasive and the nickel-plated layer is set as friction contact, and the friction coefficient is 0.1 [8]. Considering the difference of material properties between diamond and nickel and the judgment basis of the abrasive shedding which is the deformation of the nickel-plated layer, the diamond abrasive is set as a rigid body in this analysis and the C3D4 linear tetrahedral element is used to mesh the model. Additionally, the mesh refinement of the nickel-plated layer around the diamond abrasive is carried out to reflect the variation of stress gradient in the finite element model, which can ensure the

accuracy of finite element analysis. Based on the grid independence analysis, the finite element model of the diamond abrasive and the nickel-plated layer established in this paper is shown in Fig. 6, and the specific parameters are shown in Table 2.

3.2 Setting of residual stress in finite element model

The diamond abrasive is embedded and coated on the surface of the electroplated diamond wire saw by the nickel-plated layer. The electroplating process of a diamond wire saw, as described in Section 2.1, mainly includes pre-plating, sanding, and thickening. Due to the difference in the lattice constant and thermal expansion coefficient of the plating layer and the substrate, as well as the influence of the surface state of the substrate on the crystallization of the plating layer, the residual stress will be generated in the nickel-plated layer. According to the measurement results in Section 2.2, the residual stress in the nickel-plated layer formed by the composite electroplating process is compressive stress. Generally, the residual compressive stress will be decreased with the increase of thickness of the nickel-plated layer [17]. So the residual compressive stress in the nickel-plated layer can be applied to the analysis model via the equivalent cooling method, which is achieved

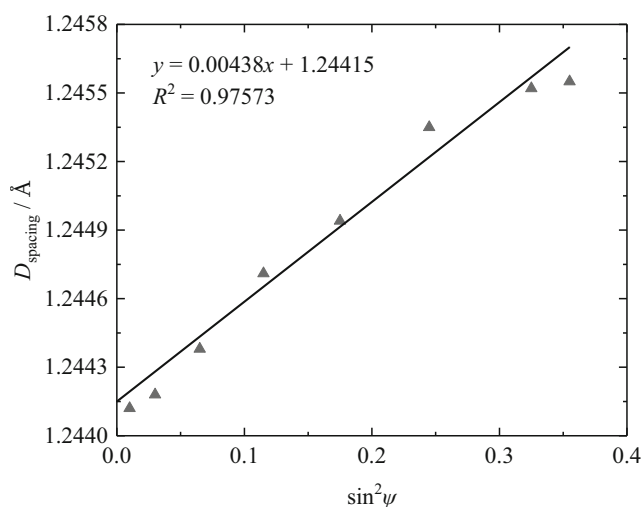
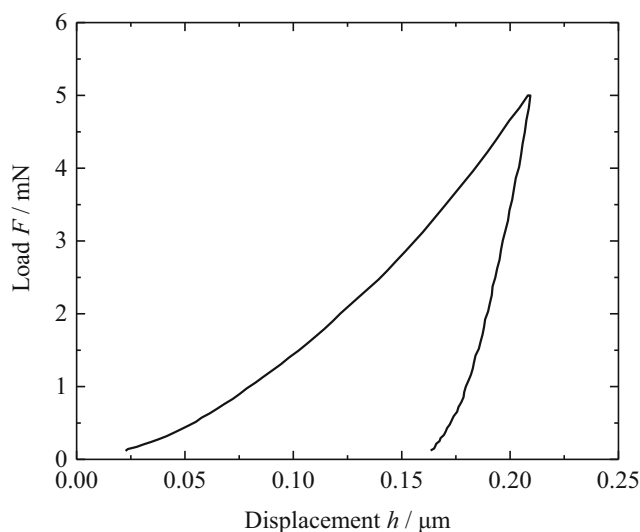
**Fig. 4** X-ray test result of residual stress in nickel-plated layer**Fig. 5** Load-displacement diagram of indentation test of nickel-plated layer

Table 2 Parameters of finite element model

Parameters	Value	
	Diamond abrasive	Nickel-plated layer
Young’s modulus (GPa)	—	166.6
Poisson’s ratio	—	0.3
Yield strength (MPa)	—	1201
Number of nodes	36586	152925

by pre-stress cooling of the finite element model without stress [12]. However, due to the complex geometry of diamond abrasive, the stress distribution in the finite element model is also too complex to be accurately added. Therefore, in this paper, the average stress σ_{AVG} in a certain area S_R on the surface of nickel-plated layer model without diamond abrasive is taken as the value of the surface residual compressive stress in the finite element model, as shown in Fig. 7(a) and (b). And then the residual compressive stress is applied to the finite element model with the abrasive via the equivalent cooling method with the same temperature difference value, as shown in Fig. 7(c). The stress field shown in Fig. 7 indicates that the residual compressive stress is decreased with the increase of thickness of the nickel-plated layer, and the value is higher at the geometric edge of the diamond abrasive, which is consistent with the results of relevant studies [12, 17].

3.3 Sawing force of single diamond abrasive

In the process of diamond wire saw slicing, the sawing force F_f of the diamond abrasive cutting edge is associated with the structure of cutting edge, workpiece material, and cutting depth, and it can be decomposed into normal force F_n and tangential force F_t calculated by Eq. (3) [18]. According to the relationship between F_n and F_t , the direction of the sawing force F_f loaded to the abrasive in the finite element model can be obtained.

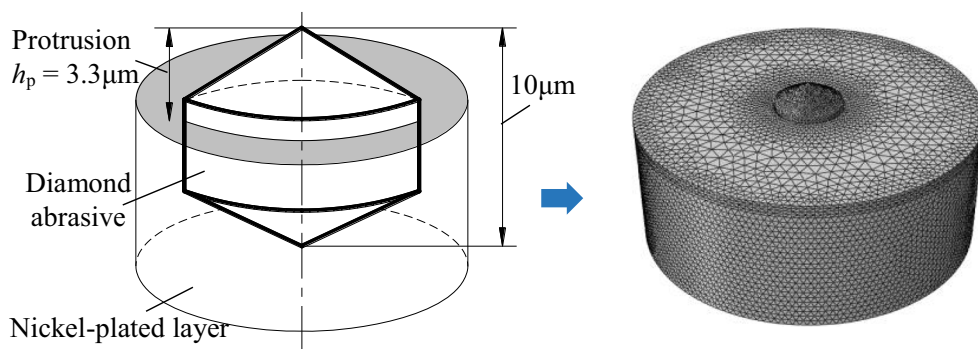
$$\begin{cases} F_n = h_a^2 H_1 \cdot \tan^2 \psi_a \left(\frac{\pi}{2} - \mu \cos \psi_a \int_0^{\frac{\pi}{2}} \frac{\sin \phi}{\sqrt{1 - \sin^2 \phi \cos^2 \psi_a}} d\phi \right) \\ F_t = h_a^2 H_1 \cdot \tan \psi_a \left(1 + \frac{\mu}{\cos \psi_a} \int_0^{\frac{\pi}{2}} \sqrt{1 - \sin^2 \phi \cos^2 \psi_a} d\phi \right) \end{cases} \quad (3)$$

where ψ_a is the half-included angle of diamond abrasive, H_1 is the hardness of workpiece material, h_a is the cutting depth of single abrasive, and μ is the friction coefficient between the diamond abrasive and the workpiece. If the sawing force loaded to the abrasive is large enough so that the deformation of the nickel-plated layer reaches a critical value, there will be an obvious gap between the nickel-plated layer and the diamond abrasive, which will make the abrasive shed, as shown in Fig. 8.

4 Results and discussions of finite element analysis

In the finite element analysis model, the stress and deformation in the nickel-plated layer are generated via applying the load corresponding to the sawing force to the diamond abrasive, as shown in Fig. 9. When the plastic strain of the nickel-plated layer embedded with the diamond abrasive reaches 4–8%, there will be an obvious gap between the abrasive and the nickel-plated layer. In this case, it can be considered that the retention effect of the nickel-plated layer has failed, and the diamond abrasive is in the critical shedding state [12]. Therefore, it is regarded as the judgment condition of abrasive shedding that the plastic strain of the nickel-plated layer is more than 8% in this paper. At this time, the sawing force applied on the abrasive is defined as the critical load of abrasive shedding F_{fmax} which is the maximum holding force of the nickel-plated layer to reflect the abrasive retention capacity. As shown in Fig. 9, the maximum plastic strain caused by the sawing force is found at the geometric edge of the extruded

Fig. 6 Finite element model of double-cone diamond abrasive embedded in nickel-plated layer



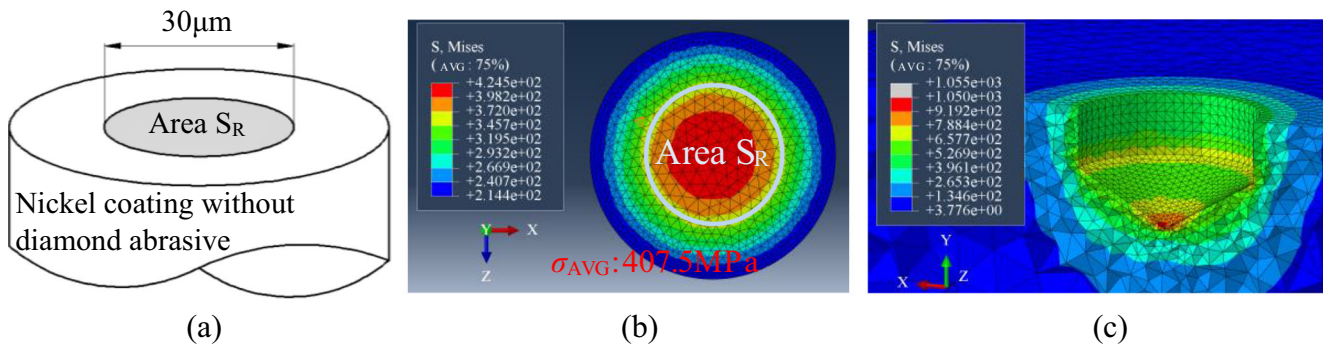


Fig. 7 Residual stress field in nickel-plated layer. **a** Schematic diagram. **b** Without diamond abrasive. **c** With diamond abrasive

side of the nickel-plated layer, which is consistent with the research conclusion of Konstanty J [12].

4.1 Influence of residual stress in nickel-plated layer on abrasive retention capacity

It is assumed that the stress in the nickel-plated layer changes linearly with temperature [19]. According to the principle of the equivalent cooling method, the residual compressive stress σ_{AVG} in the nickel-plated layer is modified via the adjustment of temperature difference of cooling. Then, the residual compressive stress field is applied to the finite element model of the nickel-plated layer according to this method proposed in Section 3.2. The sawing force is added to the diamond abrasive in the nickel-plated layer with a certain stress field. When the plastic strain of the nickel-plated layer reaches 8%, this sawing force is considered as the critical load of abrasive shedding. The influence of the residual compressive stress in the nickel-plated layer on the abrasive retention capacity is shown in Fig. 10. With the increase of the residual compressive stress in the nickel-plated layer, the critical load of diamond abrasive shedding is decreased, which will reduce the abrasive retention capacity of the nickel-plated layer so that the abrasive is easier to shed. This is because the nickel-plated layer is squeezed by the diamond abrasive loaded with sawing force to produce compressive stress. The superposition of the compressive stress produced by the external force and the

residual compressive stress generated in the electroplating process causes the plastic strain on the extruded side of the nickel-plated layer. Meanwhile, there is a certain gap on the other side. Therefore, the greater the residual compressive stress in the nickel-plated layer, the smaller the external force required to make the plastic strain of the material on the extruded side of the nickel-plated layer reach 8%, that is, the lower the abrasive retention capacity. So the existence of residual compressive stress in the nickel-plated layer is not conducive to the abrasive retention capacity [20].

4.2 Influence of hardness of nickel-plated layer on abrasive retention capacity

The hardness of the nickel-plated layer is an important parameter to reflect its mechanical properties. However, hardness cannot be directly set as a material parameter in ABAQUS. Therefore, the Vickers hardness is transformed into the yield stress of the material by Eq. (2) to accomplish the modification of the hardness of the nickel-plated layer material in the simulation, so as to obtain the critical loads of diamond abrasive shedding in the nickel-plated layer with different hardness values, as shown in Fig. 11. The higher the hardness of the nickel-plated layer, the greater the load needed to produce the same degree of plastic deformation, which will make the retention effect of the nickel-plated layer stronger so that it is more difficult for the abrasive to shed from the surface of the

Fig. 8 Sawing force of diamond abrasive

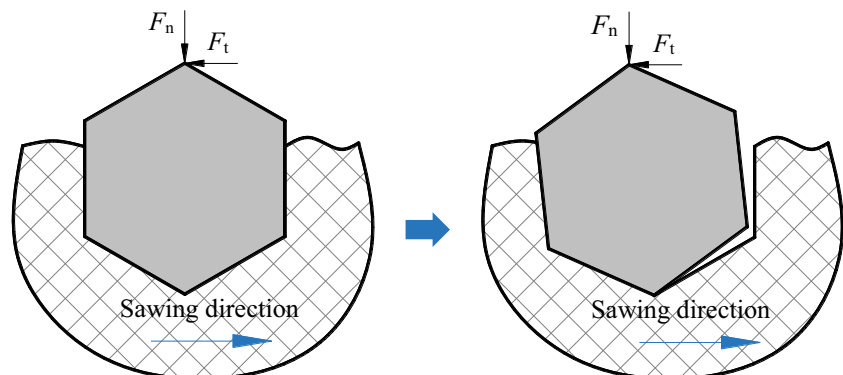
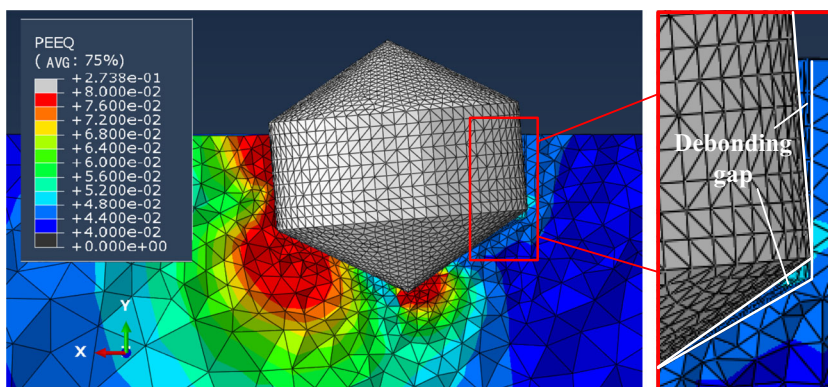


Fig. 9 Critical shedding state of diamond abrasive



nickel-plated layer. The data analysis shows that when the hardness of the nickel-plated layer is increased by about 108%, the abrasive retention capacity of the nickel-plated layer is enhanced by about 23%. On the other hand, from the overall change trend of the curve, the 3rd point of the 5 data points in Fig. 11 is different from the other 4 points. This is because that the 8% plastic strain of the nickel-plated layer caused by the critical load of abrasive shedding is far greater than the yield limit of the material, which makes the bottom of the loaded abrasive produce a displacement opposite to the load direction. When the hardness of the nickel-plated layer is at a high level (the 4th and 5th data points), the contact area between the abrasive and the nickel-plated layer is smaller than that at a low level (the 1st and 2nd data points). Due to the change of contact area, the 4th and 5th data points are below the linear fitting line of the 1st and 2nd data points. Therefore, there is a transition region where the hardness of the nickel-plated layer is at a middle level (the region where the 3rd data point is located), and the trend of curve change is relatively smooth in this region.

4.3 Influence of abrasive protrusion height on abrasive retention capacity

The protrusion height of the diamond abrasive is one of the important parameters that affect the sawing efficiency of the diamond wire saw. Generally, the reasonable protrusion height should be 1/3–1/2 of the diameter of diamond abrasive [21]. In addition, the abrasive protrusion height has a non-negligible influence on the abrasive retention capacity of an electroplated diamond wire saw. In this paper, the protrusion height values are divided into five cases, as shown in Fig. 12. The dotted line in the figure represents the upper surface of the nickel-plated layer embedded with the diamond abrasive. In the finite element analysis, the dotted line 1 ($h_{p1} = 3.3\mu\text{m}$) is taken as the initial abrasive protrusion height, and the thickness of the nickel-plated layer is gradually reduced at the interval of $0.5\mu\text{m}$ on the premise that the material properties and residual compressive stress of the nickel-plated layer are constant.

The influence of the abrasive protrusion height on the critical load of abrasive shedding is shown in Fig. 13. With the

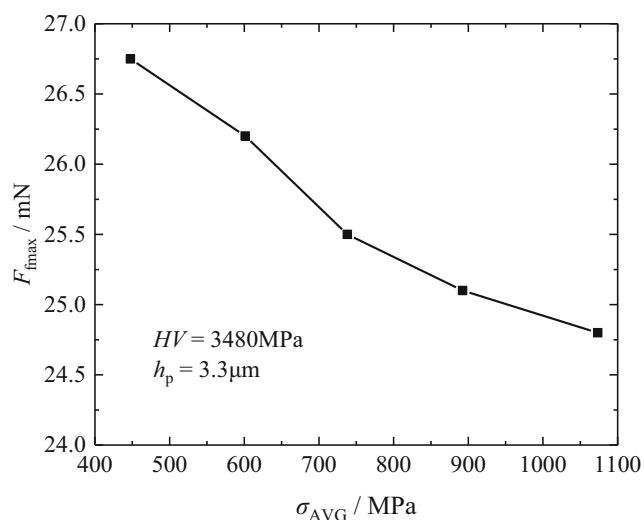


Fig. 10 Influence of residual compressive stress in nickel-plated layer on abrasive retention capacity

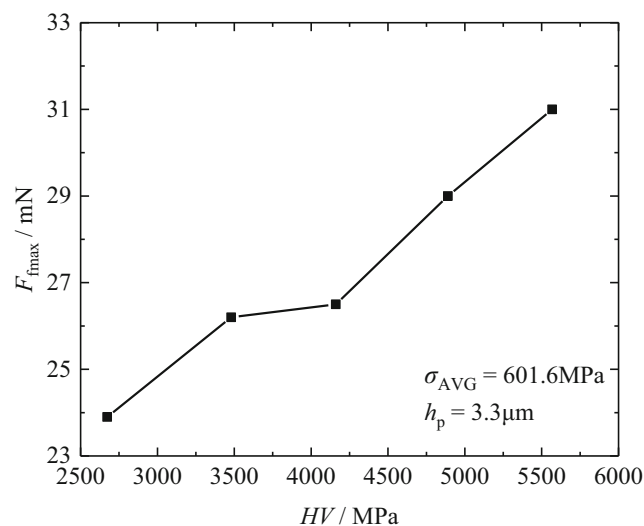


Fig. 11 Influence of hardness of nickel-plated layer on abrasive retention capacity

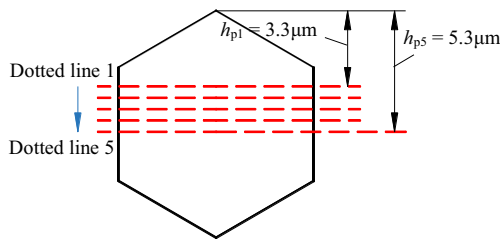


Fig. 12 Schematic diagram of protrusion height of diamond abrasive

increase of the protrusion height, the critical load of abrasive shedding is decreased, which indicates that the abrasive retention capacity of the nickel-plated layer is weakened. The data analysis shows that the abrasive retention capacity of the nickel-plated layer is decreased by about 31% when the protrusion height of double-cone diamond abrasive is increased by about 61%.

5 Abrasive shedding rate in sawing

5.1 Simulation procedure of abrasive shedding rate

The abrasive shedding on the surface of an electroplated diamond wire saw is associated with the sawing force. In order to predict the abrasive shedding rate which can directly reflect the abrasive retention capacity of the diamond wire saw in sawing, it is necessary to establish the abrasives distribution model to determine the position of the randomly distributed abrasives, so as to calculate the cutting depth of each abrasive and then obtain the abrasive sawing force [21, 22]. As shown in Fig. 14, the wire saw surface is meshed into $m \times n$ grids, where m and n are the number of grids along the circumferential direction and the axial direction respectively. The unit length of the two directions is the same to ensure that the

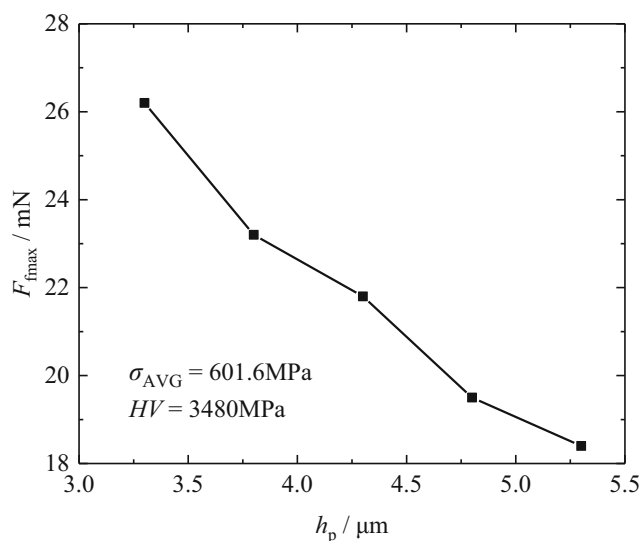


Fig. 13 Influence of abrasive protrusion height on abrasive retention capacity

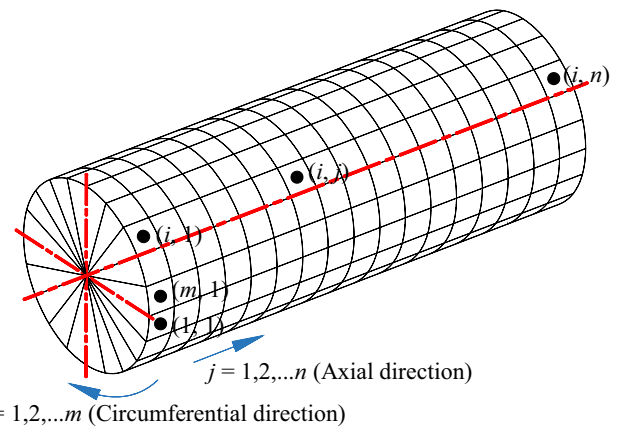


Fig. 14 Mesh model of the surface of electroplated diamond wire saw

possibility of the existence of diamond abrasive in each grid is equal, which can be expressed as

$$\frac{\pi d}{m} = \frac{l}{n} \tag{4}$$

where d is the outer diameter of the diamond wire saw and l is the contact length between the saw wire and the workpiece in sawing.

The total number of abrasives in the contact length between the saw wire and the workpiece with an abrasive density of η is

$$N = \pi \eta d l \tag{5}$$

The meshed wire can be seen as a two-dimensional zero matrix M with m rows and n columns. N non-zero numbers are randomly inserted into the matrix without repetition, and the row number i and column number j of non-zero element M_{ij} in the matrix are recorded. In the following process of defining the abrasive properties, the i th row and j th column with the non-zero numbers are calculated successively until the definition of N abrasives is completed. The position angle of

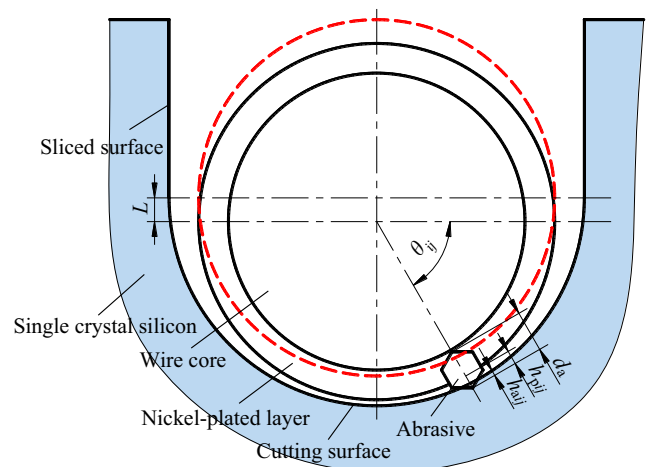
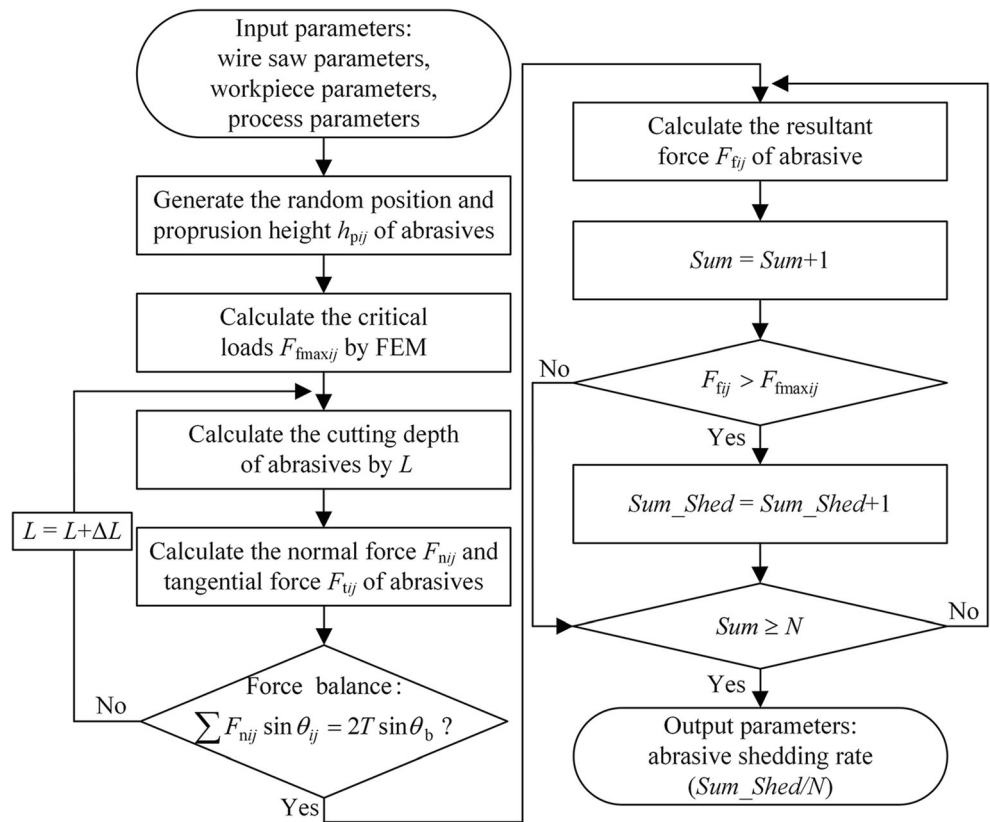


Fig. 15 Cutting depth of arbitrary abrasive on wire cross-section

Fig. 16 Simulation procedure of abrasive shedding rate



abrasive is

$$\theta_{ij} = 2\pi(i-1/2)/m \tag{6}$$

The cutting depth model of arbitrary abrasive on the wire cross-section is shown in Fig. 15. In order to simplify the calculation program, the change of abrasive size is ignored in this paper. The abrasive protrusion height defined as a random one of the five height values in Section 4.3 can be expressed as

$$h_{p_{ij}} = \text{round}[(n_p-1)\text{rand}(1)]\Delta h_p + h_{p1} \tag{7}$$

where n_p is the selected number of the abrasive protrusion

height values, $n_p = 5$; Δh_p is the interval of the abrasive protrusion height values, $\Delta h_p = 0.5\mu\text{m}$; and h_{p1} is the initial abrasive protrusion height, which is 1/3 of the diameter of diamond abrasive, $h_{p1} = 3.3\mu\text{m}$.

Therefore, the cutting depth of diamond abrasive can be obtained as

$$h_{a_{ij}} = L\sin\theta_{ij} - (h_{p_{maxj}} - h_{p_{ij}}) \tag{8}$$

where L is the displacement of downward movement of the wire cross-section in the simulation and $h_{p_{maxj}}$ is the maximum abrasive protrusion height in the j th section. If $\theta_{ij} \in [\pi, 2\pi]$ or $h_{a_{ij}} \leq 0$, $h_{a_{ij}} = 0$.

Fig. 17 Schematic diagram of single crystal silicon rod sawing with diamond wire saw

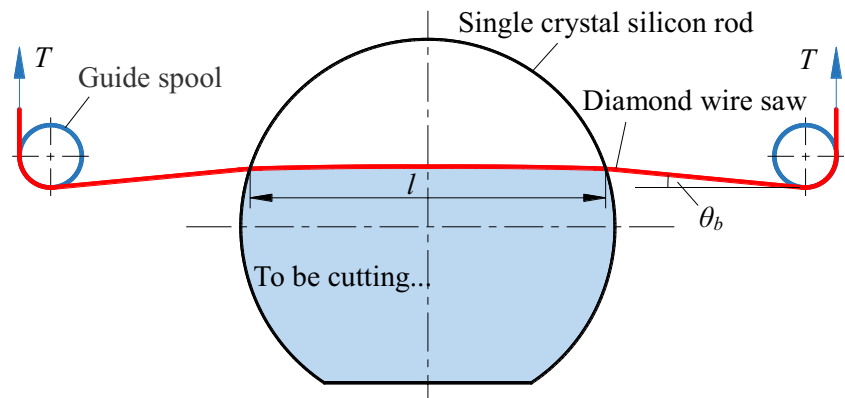


Table 3 Process parameters

Parameters	Value
Wire speed (m/min)	27.3
Feed speed (mm/min)	9
Tension force (N)	10

Substituting Eq. (8) into Eq. (3), the sawing force of the abrasive can be calculated by

$$F_{tij} = \sqrt{F_{nij}^2 + F_{tj}^2} \quad (9)$$

The simulation procedure for predicting the abrasive shedding rate shown in Fig. 16 mainly includes three steps: (1) The position and protrusion height of the abrasive are generated by the input parameters including the geometric and mechanical properties of the saw wire and the workpiece as well as the sawing parameters. Meanwhile, the critical load F_{fmaxij} of abrasive shedding with the different protrusion height of the abrasive embedded in the nickel-plated layer with a certain residual compressive stress and hardness is calculated on the basis of the finite element analysis method in Section 3; (2) the normal force and tangential force of each abrasive are solved according to the displacement L . In the slicing process, it is necessary to meet the requirement that the sum of the sawing forces in the feed direction of the abrasives is equal to the normal sawing force caused by the bending of the saw wire

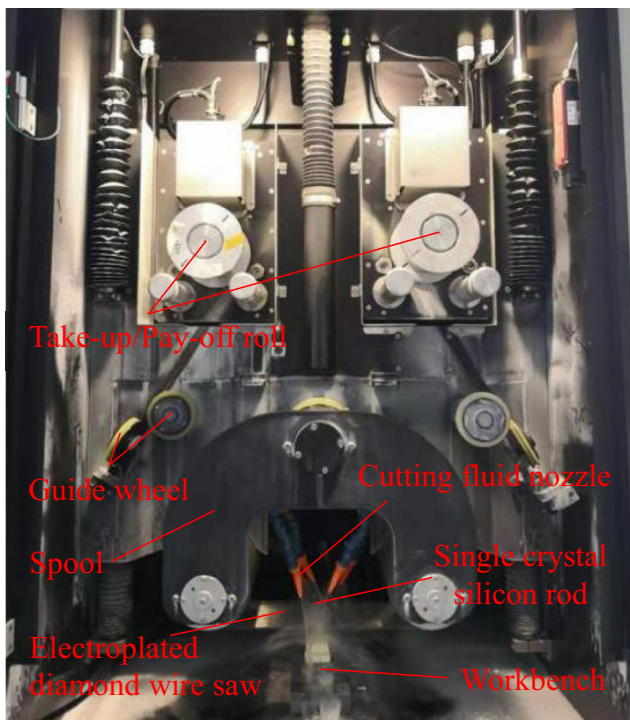


Fig. 18 Structure of the Meyer Burger RTD6800 multi-wire sawing machine

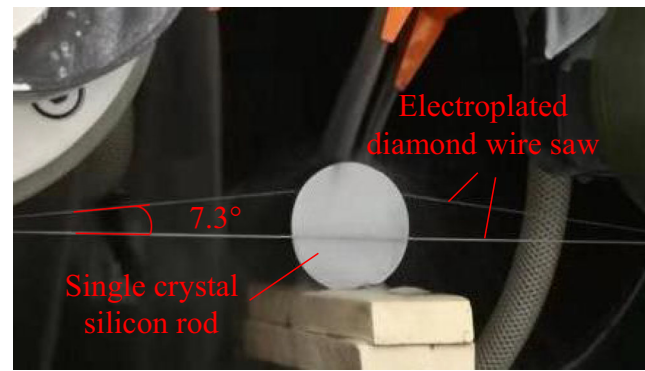


Fig. 19 Sawing process

at all times. In this paper, the abrasive shedding state is judged by the sawing force of the abrasive at the maximum bow angle θ_b in sawing. Therefore, the simulation procedure is carried out with the increase of displacement L until the sum of the normal forces on the abrasives in the feed direction $\sum F_{nij} \sin \theta_{ij}$ is balanced with the component of the tension force in this feed direction $2T \sin \theta_b$. Based on these, the sawing force F_{tij} of each abrasive is obtained; (3) taking the critical load of abrasive shedding as the limiting condition, it is considered that this abrasive will shed as long as the sawing force F_{tij} is greater than the critical load F_{fmaxij} . Then, the number Sum_Shed of abrasives that have shed can be obtained by the above judgment method to calculate the abrasive shedding rate. Due to the random distribution of the position and protrusion height of the abrasive, there will be a certain calculation deviation in the simulation procedure. Therefore, it is necessary to simulate the same set of parameters many times, and take the average value of the output results as the valid abrasive shedding rate. Furthermore, taking into account the small deflection of the wire in the contact region [23], it is assumed that this part of the diamond saw wire in contact with the workpiece in sawing

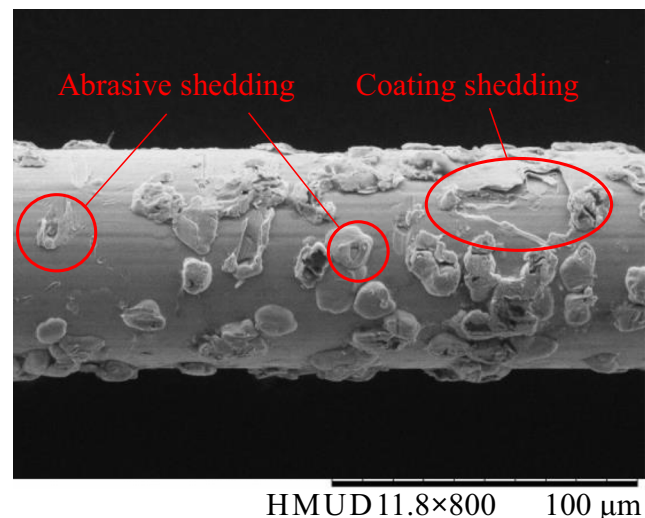
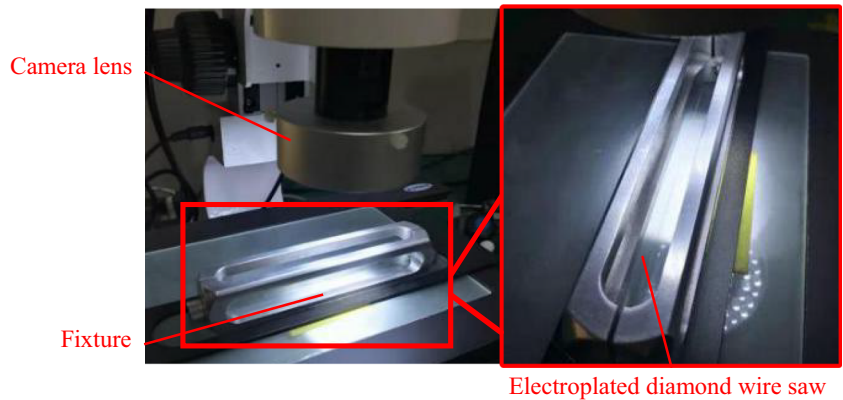


Fig. 20 Morphology of electroplated diamond wire saw after experiment

Fig. 21 Analysis test of abrasive number on the surface of electroplated diamond wire saw



will not be bent and deform as a straight line l in the paper, as shown in Fig. 17.

5.2 Sawing experiment

In this paper, the Meyer Burger RTD6800 multi-wire sawing machine is used for this sawing experiment, as shown in Fig. 18. The core wire diameter of the electroplated diamond wire saw is $65\mu\text{m}$, and the diameter of the single crystal silicon rod is 60mm . It is generally considered that the wire saw bow should not exceed 10mm in slicing [24, 25]. Therefore, it can be obtained that the bow angle should not exceed 4° during sawing according to the structure of the Meyer Burger RTD6800. However, to improve the experiment efficiency, the feed speed is increased within a certain range, and the process parameters are shown in Table 3. After a period of sawing, the bow angle of the wire saw reaches 7.3° , as shown in Fig. 19, and exposes a trend of sustained growth, which can be considered that sawing performance of the wire saw has declined significantly. The contact length between the wire and the workpiece is about 40mm in this case. At the same time, it can be seen that the surface of the wire saw after

sawing has been visibly worn via the observation of the scanning electron microscope, as shown in Fig. 20.

A KBXJ-I wire saw topography analyzer is used to analyze the abrasive shedding on the surface of the electroplated diamond wire saw before and after the experiment, as shown in Fig. 21. This device is based on the image detection method to measure the number and protrusion height values of abrasives. There are 10 analysis regions in this measurement, and the total length of measurement is 15mm . For this detection equipment, the cutting edge rate is calculated by the number of the abrasives whose cutting edge height is greater than $3\mu\text{m}$. The results of measurement show that the abrasive cutting edge rate is 288.9 abrasives/mm before sawing and 204.8 abrasives/mm after sawing. So, it can be obtained that the actual abrasive shedding rate is 29.4% in the above experiment.

Furthermore, based on the simulation procedure of abrasive shedding rate described in the previous section, it can be concluded that the theoretical abrasive shedding rate of the wire saw surface after sawing is 24.6% ($\pm 1.55\%$) by the input parameters that are shown in Table 4. The relative error between the actual abrasive shedding rate and the theoretical calculation value is about 16.3% .

Table 4 Input parameters in simulation

Parameters	Value
Wire outer diameter d (μm)	90
Density η (abrasives/ mm^2)	300
Half taper angle of abrasive ψ_a ($^\circ$)	76.903
Abrasive diameter d_a (μm)	10
Hardness of nickel-plated layer HV (MPa)	3483
Residual compressive stress of nickel-plated layer σ_{AVG} (MPa)	601.6
Hardness of silicon H_1 (GPa)	10
Friction coefficient between abrasive and workpiece μ	0.2
Length of contact between wire and workpiece l (μm)	40×10^3
Tension force T (N)	10
Wire bow angle θ_b ($^\circ$)	7.3

6 Conclusion

- (1) A finite element analysis method is established to study the abrasive retention capacity on the surface of an electroplated diamond wire saw. The residual stress in the nickel-plated layer can be applied by the equivalent cooling method.
- (2) The residual stress on the surface layer of the nickel-plated layer is compressive stress. The abrasive retention capacity can be enhanced through the decrease of the residual compressive stress and the abrasive protrusion height as well as the increase of the hardness of the nickel-plated layer. And with the increase of hardness by 108% and the decrease of the abrasive protrusion height by 61% , the abrasive retention capacity is increased by 23% and 31% , respectively.

- (3) It is reasonable for the calculation program of the abrasive shedding rate developed based on the results of finite element analysis in this paper, which has been verified through the single crystal silicon sawing experiment.

Availability of data and materials All data generated or analyzed during this study are included in this published article.

Author contribution Jintao Zheng: writing — original draft, writing — review and editing, investigation, methodology. Qian Xie: writing — original draft, numerical simulations. Peiqi Ge: conceptualization, funding acquisition, project administration, supervision. Jianfeng Meng: methodology, software and editing. Wenbo Bi: formal analysis, validation and experiment.

Funding This work was supported by the National Natural Science Foundation of China (No.51775317); and the Key Research and Development Program of Shandong Province (No.2019JZZY020209).

Declarations

Ethics approval and consent to participate Not applicable.

Consent for publication The consent to submit this paper has been received explicitly from all co-authors.

Competing interests The authors declare no competing interests.

References

- Yu X, Wang P, Li X, Yang D (2012) Thin Czochralski silicon solar cells based on diamond wire sawing technology. *Sol Energy Mater Sol Cells* 98:337–342. <https://doi.org/10.1016/j.solmat.2011.11.028>
- Gao Y, Ge P, Zhang L, Bi W (2019) Material removal and surface generation mechanisms in diamond wire sawing of silicon crystal. *Mater Sci Semicond Process* 103:104642. <https://doi.org/10.1016/j.mssp.2019.104642>
- Huang H, Wang S, Xu X (2017) Effect of wire vibration on the materials loss in sapphire slicing with the fixed diamond wire. *Mater Sci Semicond Process* 71:93–101. <https://doi.org/10.1016/j.mssp.2017.07.010>
- Li X, Gao Y, Yin Y, Wang L, Pu T (2020) Experiment and theoretical prediction for surface roughness of PV polycrystalline silicon wafer in electroplated diamond wire sawing. *J Manuf Process* 49:82–93. <https://doi.org/10.1016/j.jmapro.2019.11.022>
- Li H, Gao Y, Ge P, Bi W, Zhang L (2020) Study on process parameters of fabrication fine diameter electroplated diamond wire for slicing crystalline silicon solar cell. *Int J Adv Manuf Technol* 106:3153–3175. <https://doi.org/10.1007/s00170-019-04860-2>
- Scott PM, Nicholas M, Dewar B (1975) The wetting and bonding of diamonds by copper-base binary alloys. *J Mater Sci* 10:1833–1840. <https://doi.org/10.1007/BF00754470>
- Levin E, Gutmanas EY (1990) Solid-state bonding of diamond to Nichrome and Co-20wt% W alloys. *J Mater Sci Lett* 9:726–730. <https://doi.org/10.1007/BF00721815>
- Romanski A, Lachowski J, Konstanty J (2006) Diamond retention capacity: evaluation of stress field generated in a matrix by a diamond crystal. *Ind Diam Rev* 66:43–45. <https://www.researchgate.net/publication/275956460>
- Zhao X, Duan L, Chikhotkin VF, Weng H (2015) Summary on holding force of metallic matrix to diamond. *Diam Abras Eng* 35: 41–46, 50. <https://doi.org/10.13394/j.cnki.jgszz.2015.6.0009>
- Webb SW (1999) Diamond retention in sintered cobalt bonds for stone cutting and drilling. *Diam Relat Mater* 8:2043–2052. [https://doi.org/10.1016/S0925-9635\(99\)00167-3](https://doi.org/10.1016/S0925-9635(99)00167-3)
- Xu J, Sheikh AH, Xu C (2017) 3-D finite element modelling of diamond pull-out failure in impregnated diamond bits. *Diam Relat Mater* 71:1–12. <https://doi.org/10.1016/j.diamond.2016.11.006>
- Konstanty J, Romanski A (2014) Numerical analysis of diamond retention in cobalt and a copper-base alloy. *Arch Metall Mater* 59: 1457–1462. <https://doi.org/10.2478/amm-2014-0247>
- Noyan IC, Cohen JB (1987) Residual stress-measurement by diffraction and interpretation. Springer-Verlag Inc, New York
- Tekkaya EA (2001) Improved relationship between Vickers hardness and yield stress for cold formed materials. *Steel Res* 72:304–310. <https://doi.org/10.1002/srin.200100122>
- Mahmoud T, Tamaki J, Yan J (2003) Three-dimensional shape modeling of diamond abrasive grains measured by a scanning laser microscope. *Key Eng Mater* 238-239:131–136. <https://doi.org/10.4028/www.scientific.net/kem.238-239.131>
- Ge M, Wang P, Bi W, Ge P (2021) Fabrication of thin resin-bonded diamond wire and its application to ductile-mode wire sawing of mono-crystalline silicon. *Mater Sci Semicond Process* 126:105665. <https://doi.org/10.1016/j.mssp.2021.105665>
- Hadian SE, Gabe DR (1999) Residual stresses in electrodeposits of nickel and nickel-iron alloys. *Surf Coat Technol* 122:118–135. [https://doi.org/10.1016/S0257-8972\(99\)00328-X](https://doi.org/10.1016/S0257-8972(99)00328-X)
- Wang P, Ge P, Gao Y, Bi W (2017) Prediction of sawing force for single-crystal silicon carbide with fixed abrasive diamond wire saw. *Mater Sci Semicond Process* 63:25–32. <https://doi.org/10.1016/j.mssp.2017.01.014>
- Chen S, Liu L, Liu P, Ma J, Chen G (2009) Theoretical and experimental study on relationship between stress-strain and temperature variation. *Sci China Ser D-Earth Sci* 52(11):1825–1834. <https://doi.org/10.1007/s11430-009-0183-z>
- Chen J, Mu D, Liao X, Huang G, Huang H, Xu X, Huang H (2018) Interfacial microstructure and mechanical properties of synthetic diamond brazed by Ni-Cr-P filler alloy. *Int J Refract Met Hard Mater* 74:52–60. <https://doi.org/10.1016/j.ijrmhm.2018.03.005>
- Liu T, Ge P, Gao Y, Bi W (2017) Depth of cut for single abrasive and cutting force in resin bonded diamond wire sawing. *Int J Adv Manuf Technol* 88:1763–1773. <https://doi.org/10.1007/s00170-016-8896-6>
- Chung C, Tsay GD, Tsai MH (2014) Distribution of diamond grains in fixed abrasive wire sawing process. *Int J Adv Manuf Technol* 73(9-12):1485–1494. <https://doi.org/10.1007/s00170-014-5782-y>
- Lin Z, Huang H, Xu X (2019) Experimental and simulational investigation of wire bow deflection in single wire saw. *Int J Adv Manuf Technol* 101:687–695. <https://doi.org/10.1007/s00170-018-2919-4>
- Zhu L, Kao I (2005) Galerkin-based modal analysis on the vibration of wire-slurry system in wafer slicing using a wiresaw. *J Sound Vib* 283:589–620. <https://doi.org/10.1016/j.jsv.2004.04.018>
- Meißner D, Schoenfelder S, Hurka B, Zeh J, Sunder K, Koepge R, Wagner T, Grün A, Hagel HJ, Moeller HJ, Schwabe H, Anspach O (2014) Loss of wire tension in the wire web during the slurry based multi wire sawing process. *Sol Energy Mater Sol Cells* 120:346–355. <https://doi.org/10.1016/j.solmat.2013.05.047>

Publisher's note Springer Nature remains neutral with regard to jurisdictional claims in published maps and institutional affiliations.